IEICE TRANS. FUNDAMENTALS, VOL.E99–A, NO.7 JULY 2016

PAPER

Performance Evaluation of an Improved Multiband Impulse Radio UWB Communication System Based on Sub-Band Selection

Lin QI[†a)], ***Nonmember and*** **Masaaki KATAYAMA**[††b)], ***Fellow***

SUMMARY Performance evaluation of an improved multiband impulse radio ultra-wideband (MIR UWB) system based on sub-band selection is proposed in this paper. In the improved scheme, a data mapping algorithm is introduced to a conventional MIR UWB system, and out of all the sub-bands, only partial ones are selected to transmit information data, which can improve the flexibility of sub-bands/spectrum allocation, avoid interference and provide a variety of data rates. Given diagrams of a transmitter and receiver, the exact bit error rate (BER) of the improved system is derived. A comparison of system performance between the improved MIR UWB system and the conventional MIR UWB system is presented in different channels. Simulation results show that the improved system can achieve the same data rate and better BER performance than the conventional MIR UWB system under additive white Gaussian noise (AWGN), multipath fading and interference coexistence channels. In addition, different data transmission rates and BER performances can be easily achieved by an appropriate choice of system parameters.

key words: *multiband impulse radio UWB, sub-band selection, data mapping algorithm, interference avoidance, prolate spheroidal wave function*

1. Introduction

Impulse radio ultra-wideband (IR-UWB) communication [1], [2] using ultra-short pulses to convey information is a promising candidate for the establishment of future high-data rate indoor short-range wireless communications. UWB can also facilitate wireless communication systems with low complexity, low power consumption and high system capacity. Researchers have paid great attention to find a new UWB transmission method with better performance and a higher data transmission rate.

Paquelet originally proposed the idea of MIR UWB communication in 2004, and presented a simple noncoherent transceiver providing a high data rate with impulse radio in [3], [4]. According to this structure, on-off keying (OOK) and noncoherent energy detection were adopted for low-cost and relaxed channel estimation, and the allocated UWB frequency range (3.1–10.6 GHz) was divided into multiple sub-bands using a bandpass filter bank. The information bits were conveyed by the time-domain pulses corresponding to each sub-band (i.e., bits were transmitted on parallel multiple sub-bands). Improvement of the data transmission rate and system feasibility were also demonstrated.

Later, Mittelbach revised the system scheme in [5], where a highly flexible and scalable MIR UWB architecture for high date rates was described and evaluated. This scheme is a multiband system employing a noncoherent energy detector with an oscillator bank, OOK modulation, and convolutional channel coding. Simulation results showed satisfactory system performance for different data rates and channel conditions. The authors also pointed out the possibility of data rates on the order of several hundred Mbps up to almost a Gbps by extending the basic single-band structure to a multiband one, and adaptation to special spectrum mask or suppression of narrowband interference can be realized by switching on or off particular sub-bands.

However, the performance of OOK and noncoherent energy detection are suboptimal, and the design of a filter bank or oscillator bank with a specific bandwidth and allowed spectrum for multiple sub-bands would increase the complexity and difficulty of system implementation. Switching on or off some sub-bands would also have an impact upon the data transmission rate.

Moorfeld studied the MIR UWB system with M-PAM modulation and proposed an optimization method for the amplitude threshold using an energy detection receiver to increase data rate further [6]. But this method only works well in good channel conditions, and the BER performance worsens as the value of M increases.

A new MIR UWB scheme using prolate spheroidal wave function (PSWF) [7] pulses was proposed in [8], [9]. Because of the orthogonality and band limited characteristics of PSWF pulses, the filter bank was omitted in this scheme to decrease the system complexity. The feasibility of the system with TH-PPM and a Rake receiver was demonstrated and the BER performance under different channel conditions was also simulated and analyzed.

In the MIR UWB systems mentioned above, the frequency band allocated by FCC is entirely or mostly occupied, and all sub-bands are selected simultaneously to improve the data transmission rate, significantly decreasing the flexibility of the spectrum configuration, and increasing the requirement for orthogonality between each sub-band. As there are various wireless communication systems and services implementing a wide range of data transmission rates and qualities of service, the fixed spectrum or sub-band allocation in the conventional MIR UWB system cannot meet these requirements. Thus, an improved MIR UWB system based upon sub-band selection is proposed in this paper to

Manuscript received October 2, 2015.
Manuscript revised February 23, 2016.

[†]The author is with the College of Information and Communication Engineering, Harbin Engineering University, Harbin, 150001, China.
[††]The author is with Institute of Materials and Systems for Sustainability, Nagoya University, Nagoya-shi, 464-8603, Japan.
a) E-mail: qilin@hrbeu.edu.cn (Corresponding author)
b) E-mail: katayama@nagoya-u.jp

DOI: 10.1587/transfun.E99.A.1446

solve the above-mentioned problems. The improved system is based on a MIR UWB system using PSWF pulse for its advantages of orthogonality and bandwidth control. According to this scheme, r sub-bands are to be selected from all L sub-bands dynamically using a mapping algorithm to transmit information data, which can provide different data rates and enhance the flexibility of sub-band selection and spectrum allocation.

This paper is organized as follows. Section 2 briefly describes the MIR UWB system using PSWF pulses. In Sect. 3, a brief introduction to mapping algorithm theory is provided firstly, and then a detailed description of the improved MIR UWB system based on sub-band selection including the transmitter and receiver is presented. Simulation results and discussion are presented in Sect. 4. Section 5 contains the conclusions and some ideas for future work.

2. MIR UWB System Using PSWF

The concept of a MIR UWB system using PSWF pulse was presented in [8], [9]. The scheme proposed there is a kind of parallel structure based on a multiband PSWF pulse generator and a basic single-band UWB system.

2.1 Transmitter

The transmitter of the MIR UWB system is shown in Fig. 1, where a pulse covering 3.1–10.6 GHz generated by a pulse generator is split into L sub-bands in a bank of L adjacent bandpass filters. Simultaneously, transmitted binary bits are serially generated and afterwards parallelized and subjected to pulse amplitude modulation (PAM) or pulse position modulation (PPM) on each sub-band/branch independently. After modulation, L-modulated sub-band pulses from each branch are added together to form the transmitted MIR UWB signal, later amplified and transmitted through an UWB antenna.

If we substitute a multiband PSWF pulse generator for the multiband pulse generator as shown in Fig. 1, the system would be a MIR UWB system using PSWF pulses, referred to as the conventional MIR UWB system in this paper. In this scheme, the allocated UWB frequency range is divided into L sub-bands with equal bandwidth B, and each sub-band corresponds to a specific PSWF pulse $p_i(t)(i = 1, 2, ..., L)$. The PSWF pulse has the characteristic of biorthogonality in time and frequency domains, and its pulsewidth and band width can be controlled simultaneously and easily to fulfill the regulation requirements of FCC. The spectrum allocation of six sub-bands and their pulses in the time domain are illustrated in Fig. 2 and Fig. 3.

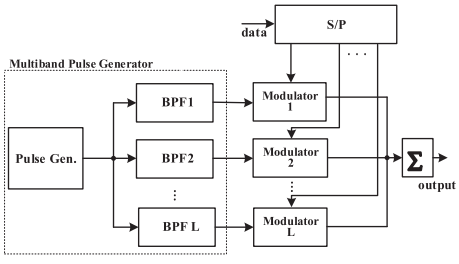

Fig. 1 Transmitter of MIR UWB system.

2.2 Receiver

The receiver of MIR UWB system is based upon L parallel coherent detectors, each having a bandpass filter (BPF), a correlator, and a decision module, as shown in Fig. 4. A specific bank of bandpass filters with no power division effect splits the received signal into L sub-bands as for the transmitter. The received signal is correlated with each of L templates first, and then sent to the decision module individually. In this paper, an ideal situation is assumed and we don't consider the effect that RF devices have upon transmitted pulses. We assume that there are no distortions during all the process and the waveforms of the received signals are the same as those transmitted, and thus the correlate templates can be generated by the same pulses as used in the transmitter. Consequently, the transmitted data bits can be detected either by soft-decision or by hard-decision. Finally, the output data are obtained using a parallel-to-serial converter.

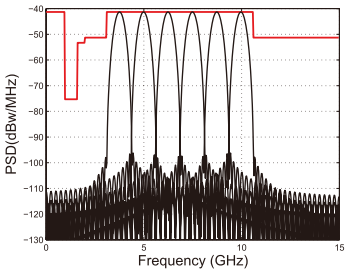

Fig. 2 Spectrum allocation of six sub-bands.

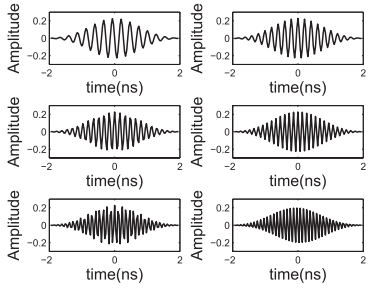

Fig. 3 Six sub-band pulses in the time domain.

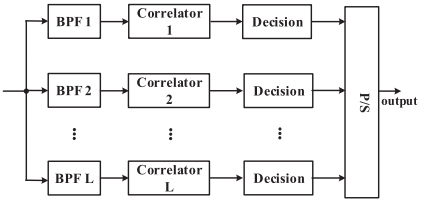

Fig. 4 Receiver of MIR UWB system.

If we use the PSWF pulse as a sub-band pulse at the transmitter, then because of the biorthogonality of PSWF pulses, the L sub-band pulses would be orthogonal in both the time and frequency domains. Therefore, no bank of bandpass filters is needed at the front end of the receiver of the conventional MIR UWB system.

3. The Improved MIR UWB System Based on Sub-Band Selection

3.1 Introduction to Mapping Algorithm Theory

The improved MIR UWB system based on sub-band selection can provide various data transmission rates using a data mapping algorithm, called r-combination mapping algorithm [10], [11], according to the following two theorems.

Theorem 1 *(from Ref. [11]) When a combination of r elements is arbitrarily selected from a set of n different elements, if the combination serial number N_d of a certain r-combination based on numerical order is known, the elements $a_i (1 \le i < r)$ in this combination can be confirmed by*

$$\min_{\{a_i\}} C_{n-a_i}^{r-i+1} \le C_n^r - N_d - \sum_{t=1}^{i-1} C_{n-a_i}^{r-t+1}, \tag{1}$$

where $\min_{\{a_i\}}$ *denotes the possible minimum value of* a_i.

Theorem 2 *(from Ref. [11]) Selecting a combination of r elements arbitrarily from a set of n different elements, when the elements in the r-combination are $a_1, a_2, ..., a_r$, then the combination serial number N_d based on numerical order can be confirmed by*

$$N_d = a_r - a_{r-1} + \sum_{t=0}^{r-2} (C_{n-a_i}^{r-t} - C_{n+1-a_{i+1}}^{r-t}), \tag{2}$$

where $a_0 = 0$.

According to Theorems 1 and 2, the uniqueness of element selection and serial number can be guaranteed.

The mapping algorithm used here has the same basic principle as that in [12], in which the PN sequences for simultaneous parallel transmission are selected by the R-out-of-M combinations among a set of pre-assigned PN sequences. While in this paper, sub-band pulses for transmission are selected by the r-out-of-L combinations among a set of basic sub-band pulses. Using this mapping algorithm, we can improve the data transmission rate as well as the variety of the data transmission rates in the improved MIR UWB system, and interference avoidance ability can also be improved by random sub-band selection. Additionally, binary pulse amplitude modulation is adopted in this paper, which is a special case of reference [12]. Other researches on the parallel combinatorial spread spectrum system using this mapping algorithm for its properties and applications are presented in [13]–[15].

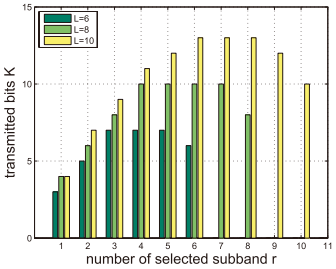

Fig. 5 Relationship between L, r and K.

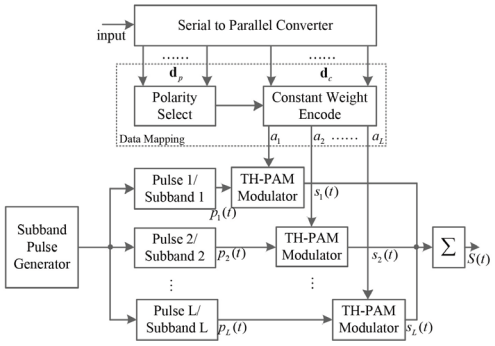

Fig. 6 Transmitter block diagram of the improved MIR UWB system.

In our improved MIR UWB system, r sub-band pulses are selected from out of a total of L (using Theorem 1) and transmitted at the transmitter. In addition, considering the two polarities of the selected pulses, there will be $2^r C_L^r$ transmission patterns. Thus, the transmission bits can be calculated by

$$K = r + [\log_2(C_L^r)] \quad \text{(bits)}, \tag{3}$$

where $[x]$ indicates the maximal integer which is less than or equal to x.

From Eq. (3), K bits can be sent at the same time, which would realize a high or low data transmission rate with different values of r and L. Figure 5 displays the relationship between L, r, and K for achieving different data transmission rates.

3.2 Transmitter Model

The transmitter block diagram of the improved MIR UWB system is illustrated in Fig. 6.

At the transmitter, K binary information bits $\mathbf{d} = [d_1, d_2, ..., d_K]$, should first be converted from serial data bits into parallel ones, and then divided into two parts $\mathbf{d_c}$ and $\mathbf{d_p}$. $\mathbf{d_c} = [d_1, d_2, ..., d_{K-r}]$ is the set of the first $(K - r)$ bits in $\mathbf{d}$, and will decide the serial number of selected pulse/sub-band according to the data mapping algorithm. $\mathbf{d_p} = [d_{K-r+1}, d_{K-r+2}, ..., d_K]$ is the set of the last r bits in $\mathbf{d}$, and will decide the polarities of the selected pulses. This mapping procedure can be regarded as a constant weight encoding, because after data mapping the output data have the same length L and same code weight r. We describe this

procedure as follows:

1) Convert $\mathbf{d_c} = [d_1, d_2, ..., d_{K-r}]$ into decimal number N_d (called the combination serial number):

$$N_d = d_1 2^0 + d_2 2^1 + ... + d_{K-r} 2^{K-r-1}. \quad (4)$$

2) Select r sub-bands/pulses according to Eq. (1). The matrix of chosen sub-bands/pulses is $\mathbf{C}_{1\times L} = [c_1, c_2, ..., c_L], c_i \in \{0, 1\}, i = 1, 2, ..., L$. When $c_i = 1$, the i-th sub-band/pulse is selected; when $c_i = 0$, the i-th sub-band/pulse is not selected. Thus, there are only r atoms equal to 1 in $\mathbf{C}$, and the others are equal to 0.

3) Confirm the polarity of the selected sub-band pulses by $\mathbf{d_p} = [d_{K-r+1}, d_{K-r+2}, ..., d_K]$

$$q_i = \begin{cases} (-1)^{d_{K-r+j}} & (j = 1, 2, ..., r) \quad c_i = 1 \\ 0 & c_i = 0, \end{cases} \quad (5)$$

where q_i is the polarity factor of i-th sub-band pulse.

4) Export mapping data $\mathbf{a} = [a_1, a_2, ..., a_L]$:

$$a_i = c_i q_i \quad (i = 1, 2, ..., L), \quad (6)$$

where a_i is the transmitted bit of the i-th sub-band.

Then, a_i is sent to the TH-2PAM modulator for the pulse amplitude to be modulated on each branch independently. Using the time-hopping code can avoid the appearance of the line spectrum, and smooth-out the power spectrum of the modulated signal. Finally, the modulated signal of each branch can be represented as

$$s_i(t) = \sqrt{E_{TX}} \sum_{n=-\infty}^{+\infty} \sum_{j=nN_s}^{(n+1)N_s-1} a_i p_i(t - jT_f - C_{i,j}T_c), \quad (7)$$

where $i = 1, 2, ..., L$. $\sqrt{E_{TX}}$ indicates the amplitude of the transmitted pulse. N_s indicates the number of pulses per information bit. a_i indicates the transmitted data of the i-th sub-band. $p_i(t)$ denotes the PSWF pulse of the i-th sub-band with pulse duration T_p, and with $\int_{-\infty}^{+\infty} p_i^2(t)dt = 1$. T_f indicates the pulse repetition time and $T_f \geq T_p$. $C_{i,j}$ is the j-th time-hopping code in the i-th branch with periodicity N_p and $C_{i,j} \in [0, N_h)$, N_h is the cardinality of the time hopping code, and T_c is the time shift of each time hopping chip.

According to the data mapping algorithm, there are only r output signals from all the L branches. By adding them together, we will obtain the transmitted signal as follows:

$$\begin{aligned} S(t) &= \sum_{i=1}^{L} s_i(t) \\ &= \sum_{i=1}^{L} \sqrt{E_{TX}} \sum_{n=-\infty}^{+\infty} \sum_{j=nN_s}^{(n+1)N_s-1} a_i p_i(t - jT_f - C_{i,j}T_c). \end{aligned} \quad (8)$$

Figure 7 gives an example of transmitter with 4 sub-bands/pulses. According to Eq. (3), $L = 4$, $r = 2$ and $K = 4$ bits in Fig. 7. Thus, there are only 2 sub-bands/pulses selected to transmit information. The spectrum of this example is also shown in Fig. 8.

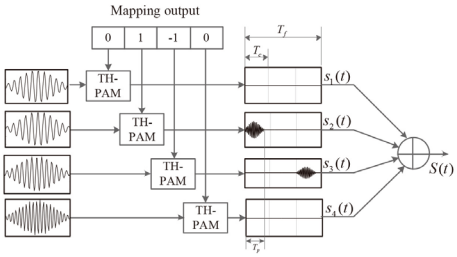

Fig. 7 Transmitter with four sub-bands.

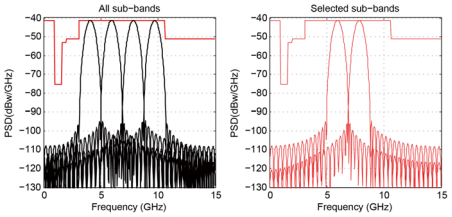

Fig. 8 Spectrum of four sub-bands and two selected sub-bands.

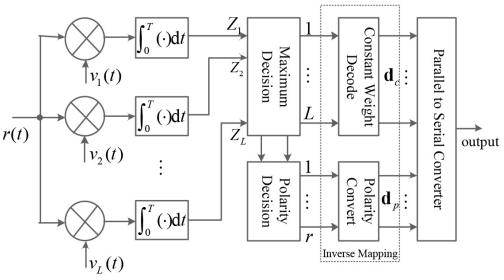

Fig. 9 Receiver block diagram of the improved MIR UWB system.

3.3 Receiver Model

The receiver block diagram of the improved MIR UWB system is illustrated in Fig. 9.

For the sake of simplicity, we assume a perfect time synchronization between transmitter and receiver, the channel is AWGN channel without multipath, so the received signal can be expressed as

$$\begin{aligned} r(t) &= S(t) + n(t) \\ &= \sum_{i=1}^{L} \sqrt{E_{TX}} \sum_{n=-\infty}^{+\infty} \sum_{j=nN_s}^{(n+1)N_s-1} a_i p_i(t - jT_f - C_{i,j}T_c) \\ &\quad + n(t), \end{aligned} \quad (9)$$

where $n(t)$ is the zero-mean additive white Gaussian noise with double-sided power spectral density $N_0/2$.

Owing to the biorthogonality of PSWF pulses, there is no filter bank needed at the receiver side to separate each sub-band pulse as in [3], [4], which decreases the complexity of the receiver.

At the receiver, the received signal is first correlated with L templates and then integrated over the time interval $N_s T_f$ separately, and the i-th template signal can be ex-

pressed as

$$v_i(t) = \sum_{j=0}^{N_s-1} p_i(t - jT_f - C_{i,j}T_c). \tag{10}$$

Additionally, there will be L output values $\mathbf{Z} = (Z_1, Z_2, ..., Z_L)$, exported from the integrators, and the i-th output value Z_i can be expressed as

$$\begin{aligned} Z_i &= \int_0^{N_sT_f} r(t)v_i(t)dt \\ &= \int_0^{N_sT_f} \sqrt{E_{TX}} \sum_{n=-\infty}^{+\infty} \sum_{j=nN_s}^{(n+1)N_s-1} a_i p_i(t - jT_f - C_{i,j}T_c) \\ &\times \sum_{j=0}^{N_s-1} p_i(t - jT_f - C_{i,j}T_c)dt \\ &+ \int_0^{N_sT_f} \sum_{m\neq i} \sqrt{E_{TX}} \sum_{n=-\infty}^{+\infty} \sum_{j=nN_s}^{(n+1)N_s-1} a_m p_m(t - jT_f - C_{m,j}T_c) \\ &\times \sum_{j=0}^{N_s-1} p_i(t - jT_f - C_{i,j}T_c)dt + N(t), \end{aligned} \tag{11}$$

where $N(t)$ is a Gaussian random variable with zero mean value and variance $N_0N_s/2$, which can be expressed as

$$N(t) = \int_0^{N_sT_f} n(t) \sum_{j=-\infty}^{+\infty} p_i(t - jT_f - C_{i,j}T_c)dt. \tag{12}$$

According to the biorthogonality of PSWF pulses, the pulse $p_i(t)$ has the characteristic

$$\int_{-T/2}^{+T/2} p_i(t)p_m(t)dt = \begin{cases} 1 & i = m \\ 0 & i \neq m. \end{cases} \tag{13}$$

Thus, Eq. (11) can be simplified to

$$Z_i = \sqrt{E_{TX}}a_iN_s + N(t). \tag{14}$$

Considering the mapping algorithm at the transmitter, only r branches have transmitted signals, thus there will be r components that contain signals in $Z_i(i = 1, 2, ..., L)$, the $L - r$ remainders are noise components.

Afterward, Z_i is put into the maximum detector to decide which branch the received signal belongs to. If $|Z_i| > |Z_m|$, $m \neq i(m = 1, 2, ..., L - r)$, the i-th sub-band pulse has been received. The probability of correct decision is

$$\begin{aligned} P_{c_i} &= P[|Z_i| > 0, |Z_i| > |Z_m|, m = 1, 2, ..., L - r, i \neq m] \\ &= \int_0^{+\infty} [p(|Z_i| > |Z_m|)]^{L-r} p(Z_i)dZ_i \\ &= \int_0^{+\infty} \left(\int_{-Z_i}^{+Z_i} \frac{1}{\sqrt{2\pi}\sigma_n} e^{-\frac{u^2}{2\sigma_n^2}} du \right)^{L-r} \frac{1}{\sqrt{2\pi}\sigma_n} e^{-\frac{(Z_i - \sqrt{E_{TX}}N_s)^2}{2\sigma_n^2}} dZ_i \\ &= \frac{1}{\sqrt{2\pi}} \int_{-\frac{\sqrt{E_{TX}}N_s}{\sigma_n}}^{+\infty} \left[1 - \mathrm{erfc}\left(\frac{x + \sqrt{E_{TX}}N_s/\sigma_n}{\sqrt{2}} \right) \right]^{L-r} e^{-\frac{x^2}{2}} dx, \end{aligned} \tag{15}$$

where Z_i is a Gaussian random variable with a mean value of $\sqrt{E_{TX}}N_s$ and variance of $N_0N_s/2$, $\mathrm{erfc}(y) = \frac{2}{\sqrt{\pi}} \int_y^{+\infty} e^{-u^2} du$.

Then, the probability of correct decision for all r branches (pulses) is given by

$$P_c = (P_{c_i})^r. \tag{16}$$

Therefore, the probability of error decision is

$$P_e = 1 - P_c = 1 - (P_{c_i})^r. \tag{17}$$

After the maximum decision, inverse mapping is adopted to recover the transmitted data as follows:

1) Confirm the serial number of the r selected sub-bands by comparing the L values in $\mathbf{Z}$, where r values will larger than others, and then sort them in numerical order as $\mathbf{z} = [z_1, z_2, ..., z_r]$.

2) Confirm the combination serial number N_d according to the results of 1) and Eq. (2).

3) Convert N_d from decimal data into binary data and obtain $\mathbf{d_c} = [d_1, d_2, ..., d_{K-r}]$.

4) Confirm the polarity factor $q_m(m = 1, 2, ..., r)$ according to $\mathbf{z}$:

$$q_m = \begin{cases} 1 & z_m > 0 \\ -1 & z_m < 0. \end{cases} \tag{18}$$

5) Recover $\mathbf{d_p} = [d_{K-r+1}, d_{K-r+2}, ..., d_K]$:

$$d_{K-r+m} = \frac{1 - q_m}{2} \quad (m = 1, 2, ..., r). \tag{19}$$

6) Combining $\mathbf{d_c}$ and $\mathbf{d_p}$, output data $\mathbf{d}$ can be obtained.

There will be $n(n \leq K)$ errors in K bits corresponding to r sub-band pulses when errors occur during the maximum decision procedure. The probability of an average occurrence of n bit errors is

$$\overline{P_n} = \sum_{n=1}^{K} nP_n = \frac{K2^{K-1}}{2^K - 1}, \tag{20}$$

where

$$P_n = \frac{C_K^n}{\sum_{j=1}^{K} C_K^j}. \tag{21}$$

Then, the bit error rate of the system is

$$P_{e_b} = \frac{1}{K} \frac{K2^{K-1}}{2^K - 1} P_e \approx \frac{1}{2} P_e. \tag{22}$$

Errors will also arise during the polarity decision because the selected pulses have two polarities, positive and negative. However, the probability of error polarity decision is far less than that of error maximum decision, and therefore it can be ignored [16].

Table 1 Simulation parameters.

Parameters	Descriptions	Value
L	Number of sub-band	12/15
B	Sub-band bandwidth	600MHz
r	Number of selected sub-band	2,4,7/2,5
N_s	Number of pulses per bit	1
T_f	Pulse repetition time	15ns
T_p	Pulse duration	4ns
T_c	Time shift of TH chip	5ns
N_h	Cardinality of TH code	3
N_p	Periodicity of TH code	12

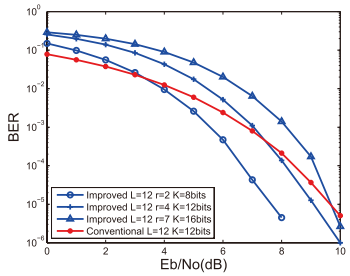

Fig. 10 BER comparison of improved and conventional MIR UWB systems.

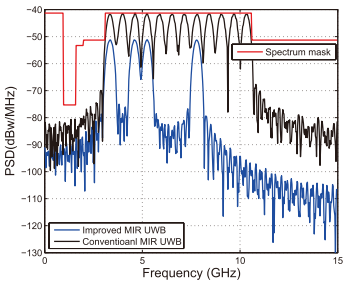

Fig. 11 Spectrum allocation of the two systems.

Table 2 Communication distance and data transmission rate.

L	r	K(bits)	R_b(Mbit/s)	D(m)
$L = 12$	2	8	533.33	12.8566
	4	12	800	9.5472
	7	16	1066.7	7.6751
$L = 15$	2	8	533.33	12.7617
	5	16	1066.7	8.3196
$L = 8$	/	8	533.33	11.4144
$L = 12$	/	12	800	9.3199
$L = 16$	/	16	1066.7	8.0242

4. Simulation Results and Discussion

In this section, the model of the improved MIR UWB system is set up by MATLAB according to Fig. 6 and Fig. 9 to evaluate the system performance. For simplified analysis, exact time synchronization is assumed. A set of orthogonal PSWF pulses is chosen for the system and each transmitted sub-band pulse has the same transmission power. TH-2PAM with bipolar pulse is adopted. Other system parameters are listed in Table 1.

Figure 10 gives the comparison results between the improved and the conventional MIR UWB systems. When $L = 12$, $r = 4$, $K = 12$ bits in the improved MIR UWB system and $L = 12$, $K = 12$ bits in the conventional MIR UWB system, these two systems have the same data transmission rate. It can be seen from the curves that, at lower E_b/N_0 the BER performance of the conventional system is better than the improved one because of the independent demodulation on each branch/sub-band. When E_b/N_0 increases, the BER performance of the improved system improves and exceeds the conventional curve after $E_b/N_0 > 7.5$ dB, because the accurate recovery of transmitted data depends upon the correct decision of all r branches, and the probability of such correct decisions improve as well as E_b/N_0 increases.

For this case, these two systems have the same data transmission rate. But during the pulse repetition time T_f, K bits are transmitted using 4 sub-band pulses in the improved system and 12 sub-band pulses in the conventional system, which can significantly decrease the number of transmitted pulses/sub-bands as well as the transmission power. This is because the full transmission power can be obtained as the product of the number of transmitted pulses and the transmission power per pulse. Figure 11 shows the spectrum allocation of these two systems.

From Fig. 10 we can also see that when we change the parameter r, the transmitted bit K will change along with it, and will transmit more or fewer bits, thereby providing different data transmission rate flexibly. This can also solve the contrary problem between decreasing pulse repetition frequency and improving transmission data rate properly. Meanwhile, when r increases, K will increase at the same time, implying that more bits will be transmitted, but the BER performance will worsen because of the contradiction between reliability and efficiency. Thus, we should choose suitable values of L or r to meet the requirements for different data transmission rates and system BER performances.

Considering the application of UWB to indoor short-range and high-data rate communication, the communication distance D and data transmission rate R_b that can be achieved by the improved and conventional MIR UWB systems are listed in Table 2. For this table, no multipath and free-space transmission are considered and the communicaiton distance D for different data transmission rate R_b can be calculated under the condition of a fixed transmission power 0.55 mW [17]. This represents the maximum output power allowed by FCC for license-free use of UWB transmission. The data transmission rate is given by $R_b = K/T_f$, where T_f and K stand for the pulse repetition time and the number of transmitted bits, respectively. With regard to communication distance, in most cases, the improved MIR UWB system has a slight advantage compared to the conventional one with the same data transmission rate.

The simulation is also performed in the multipath fading channel, and we focus only upon the system performance under ideal conditions. The intersymbol interference has not been taken into account by choosing symbol intervals larger than the channel delay spread. We also

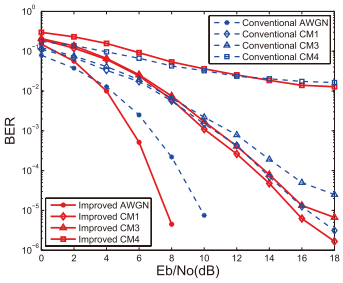

Fig. 12 BER performance comparison in different channel model (L = 12, r = 2, K = 8 bits).

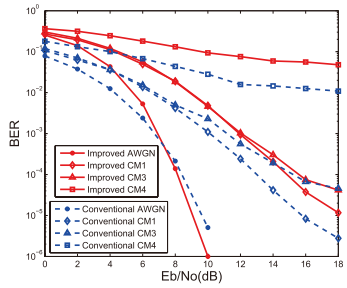

Fig. 13 BER performance comparison in different channel model (L = 12, r = 4, K = 12 bits).

assume that accurate channel estimation has already been completed, and that the receiver has already achieved a priori information about the channel impulse response. An all RAKE (A-Rake) receiver and the maximum ratio combining technique are employed to maximize the output signal-to-noise ratio. The A-Rake receiver is an ideal RAKE receiver that can collect all multipath components to guarantee the best reception performance. But the adoption of an A-Rake receiver increases the system's complexity and cost. To decrease the complexity of the receiver, a selective RAKE (S-Rake) receiver, which selects the L_s best components, and a partial RAKE (P-Rake) receiver, which combines the first arriving L_p components can be employed in place of the A-Rake receiver according to the actual requirements.

Figure 12 to Fig. 16 present the BER performances of the improved and conventional MIR UWB systems with different parameters in IEEE802.15.3a channel model. The same data transmission rate is guaranteed in these two comparison systems for each group of curves. It can be observed from Fig. 12 to Fig. 16 that the BER performances in the multipath fading channel are all worse than those in AWGN channel because of the influence of multipath fading, and they also become worse along with the channel conditions from line-of-sight (LOS) CM1 channel to no line-of-sight (NLOS) CM4 channel. In particular, in CM4 channel, the BER performances deteriorate extremely, and no reliable communication can be achieved. Thus, the BER performances in CM4 channel will not be discussed here.

In Fig. 12, the BER performances of the improved system is slightly better than that of the conventional system. However, with the increase of r (i.e., when $r = 4, 7$ in Fig. 13 and Fig. 14), the BER performances of the improved system become worse than that of the conventional ones. The increase in r implies an increase in the number of transmitted pulses, which decreases the probability of correct decisions for the maximum values of r branches simultaneously, as well as the BER performances. In addition, the ratio of the bandwidth of the selected sub-bands to the whole bandwidth becomes larger along with the increase of r, and the influence of frequency-selective fading caused by the multipath fading channel increases, worsening system performance.

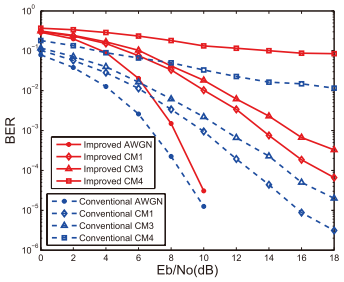

Fig. 14 BER performance comparison in different channel model (L = 12, r = 7, K = 16 bits).

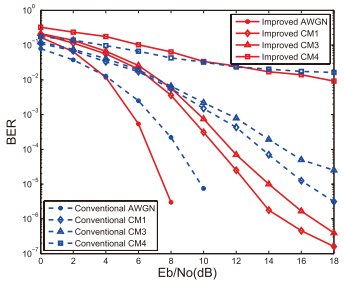

Fig. 15 BER performance comparison in different channel model (L = 15, r = 2, K = 8 bits).

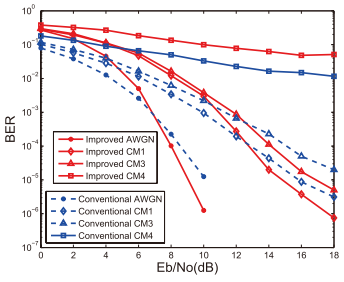

Fig. 16 BER performance comparison in different channel model (L = 15, r = 5, K = 16 bits).

It can be seen from Fig. 15 and Fig. 16 that when L = 15 and $r = 2, 5$, the improved system has the better BER performances than the conventional one and the improved system with L = 12 and $r = 2, 7$. Because the ratio of the bandwidth of the selected sub-bands to the whole bandwidth decreases along with the increase of L value, the influence of frequency-selective fading decreases as well.

As an unlicensed MIR UWB system, there will be various sources of interference from present and future ra-

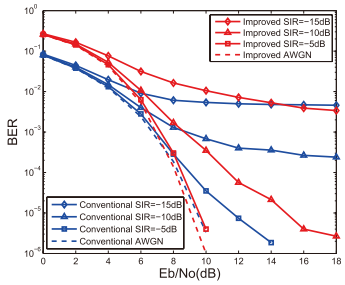

Fig. 17 BER performance comparison with interference in one sub-band.

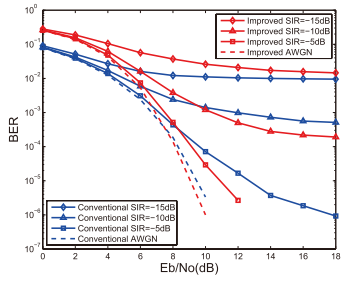

Fig. 18 BER performance comparison with interference in two sub-bands.

dio systems operating in the same frequency range of 3.1–10.6 GHz. Therefore, at the end of this section, we present a system performance simulation assuming the existence of interference. Transmission is affected by AWGN, and an OFDM signal at 4.6 GHz or 7.8 GHz with 128 subcarriers and a 600 MHz bandwidth is chosen as the source of interference. It is assumed that the OFDM interference source is always present to illustrate the impact of the interference. The BER performances of the improved and conventional MIR UWB systems with one and two interference signals are evaluated when the signal-to-interference ratio (SIR) is −15 dB, −10 dB and −5 dB. The definition of SIR is given by SIR= $10\log_{10}(P_{\mathrm{p}}/P_{\mathrm{OFDM}})$, where P_{p} denotes the signal power of a sub-band pulse and P_{OFDM} denotes the signal power of the OFDM interference signal with respect to the bandwidth of 600 GHz. The simulation results are illustrated in Fig. 17 and Fig. 18.

Figure 17 depicts the BER performance comparison with one interference signal. The central frequency of the interference is 4.6 GHz, and consequently the third sub-band is subject to interference. Figure 18 depicts the BER performance comparison with two interference signals. The central frequencies of the interferences is 4.6 GHz and 7.8 GHz, consequently, the third sub-band and the eighth sub-band are subject to interference.

It is obvious that, the existence of one or two interference sources leads to a tremendous decrease in the BER performance of both the systems. For instance, when SIR = −15 dB, these two systems cannot even work normally for their larger bit error rates at the level about 10^{-2}. While along with the increase of SIR, an asymptotic approximation to the BER curve of the interference free case (AWGN only) can be observed. When SIR = −10 dB, −5 dB, respectively, the BER performances of the improved MIR UWB system are superior to those of the conventional system in the case of large E_b/N_0.

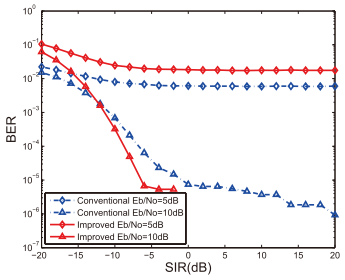

Fig. 19 BER performance via SIR with fixed E_b/N_0.

When BER is 10^{-5}, the E_b/N_0 gap between AWGN case curve and the improved MIR UWB curve is also smaller than that of the conventional MIR UWB system. Because we only select a small number of transmitted pulses/sub-bands in the improved MIR UWB system using the mapping algorithm, we can, in a sense, avoid the interfered sub-bands. That is, the interference signal will not disturb the transmitted signal at all times, but only when the interfered sub-band is selected for transmission. Thus, the improved MIR UWB system has the ability to avoid interference.

Figure 19 depicts the BER performance via varied SIR with the third sub-band subject to interference under the condition of fixed E_b/N_0 (5 dB and 10 dB). It can be seen from Fig. 19 that the two systems cannot work well when E_b/N_0 = 5 dB. Meanwhile, when E_b/N_0 = 10 dB, the BER performances improve along with the increase in SIR in both systems. Furthermore, the improved MIR UWB system has a faster improvement speed and better BER performance than the conventional MIR UWB system because of its interference avoidance ability.

5. Conclusion

In this paper, performance evaluation of an improved MIR UWB system based on sub-band selection is investigated. The improved MIR UWB system can enhance the flexibility of spectrum allocation and sub-band selection, as well as the variety of data transmission rates by selecting partial sub-bands using a mapping algorithm and a set of PSWF pulses. The transmitter and receiver structures are given and the bit error rate under AWGN channel is also derived.

Simulation results show that the BER performance of the improved MIR UWB system is better than the conventional MIR UWB system under the conditions of AWGN channel and the same data transmission rate. They also show superior BER performance in the multipath fading and interference existence channels. In addition, different requirements of data transmission rate and BER performance can be realized by suitable selection of system parameters.

Future work will be focused on the combination of er-

ror correction schemes and the improved MIR UWB system with respect to the combination method and the new system scheme.

Acknowledgement

The authors would like to thank Profs. T. YAMAZATO, H. OKADA and K. KOBAYASHI of Nagoya University for their valuable comments and suggestions. This work was supported by National Nature Science Foundation of China (No.61401115) and the Fundamental Research Funds for the Central Universities (No.HEUCF1608).

References

[1] M.Z. Win and R.A. Scholtz, "Impulse radio: How it works," IEEE Commun. Lett., vol.2, no.2, pp.36–38, 1998.
[2] L.Q. Yang and G.B. Giannakis, "Ultra-wideband communications: An idea whose time has come," IEEE Signal Process. Mag., vol.21, no.6, pp.26–54, 2004.
[3] S. Paquelet and L.M. Aubert, "An energy adaptive demodulation for high data rates with impulse radio," Proc. 2004 IEEE Radio and Wireless Conference, pp.323–326, 2004.
[4] S. Paquelet, L.-M. Aubert, and B. Uguen, "An impulse radio asynchronous transceiver for high data rates," Proc. 2004 International Workshop on Ultra Wideband Systems Joint with Conference on Ultra Wideband Systems and Technologies, pp.1–5, 2004.
[5] M. Mittelbach, R. Moorfeld, and A. Finger, "Performance of a multiband impulse radio UWB architecture," Proc. 3rd International Conference on Mobile Technology, Applications & Systems, Mobility'06, Article No. 17, 2006.
[6] R. Moorfeld and A. Finger, "Multilevel PAM with optimal amplitudes for non-coherent energy detection," 2009 International Conference on Wireless Communications & Signal Processing, pp.1–5, 2009.
[7] D. Slepian and H.O. Pollak, "Prolate spheroidal wave functions, Fourier analysis and uncertainty-I," Bell Syst. Tech. J., vol.40, no.1, pp.43–63, 1961.
[8] L.L. Chen, Z. Dou, L. Yan and Y. Lin, "Research on multiband impulse radio UWB system based on PSWF in multipath fading channel," International Journal of Signal Processing, Image Processing and Pattern Recognition, vol.6, no.6, pp.205–214, 2013.
[9] L.L. Chen, X. Yu, and Z. Dou, "Research on the performance of multiband impulse radio UWB communication system based on PSWF," J. Harbin Engineering University, vol.35, no.4, pp.1–5, 2014.
[10] X.F. Jiang, Research on key technologies of UWB communication systems based on parallel combinatory spread spectrum, Ph.D. Dissertation, Harbin Engineering University, 2012.
[11] L.L. Guo, Q. Yi, and B.M. Li, "Parallel combinatory spread spectrum communication system based on r-combinatory," Information Transmission and Access Technology, vol.33, no.4, pp.25–27, 2007.
[12] S. Sasaki, H. Kikuchi, J.K. Zhu, and G. Marubayashi, "Error rate analysis of coherent and differential multiphase parallel combinatorial spread spectrum systems," IEICE Trans. Fundamentals, vol.E80-A, no.7, pp.1196–1203, 1997.
[13] J.K. Zhu and G. Marubayashi, "Parallel combinatory SS communication," IEICE, SSTA90-23, pp.34–42, 1990.
[14] J.K. Zhu, S. Sasaki, and G. Marubayashi, "Proposal of parallel combinatory spread spectrum communication system," IEICE Trans. Commun. (Japanese Edition), vol.J74-B-II, no.5, pp.207–214, 1991.
[15] J.K. Zhu and G. Marubayashi, "Properties and application of parallel combinatory SS communication system," IEEE Second International Symposium on Spread Spectrum Techniques and Applications, pp.227–230, 1992.
[16] J.K. Zhu, CDMA communication technology, Posts and Telecom Press, 2001.
[17] L.J. Ge, L. Zhu, X.F. Yuan, and B.F. Chen, Understanding Ultra Wideband Radio Fundamentals, Publishing House of Electronics Industry, 2005.

Lin Qi received the B.S., M.S. and Ph.D. degrees in Communication Engineering, Signal and Information Processing, and Communication and Information System from Harbin Engineering University, China in 2002, 2005 and 2011, respectively. From 2002 to 2005, she was an Assistant Professor of College of Information and Communication Engineering at Harbin Engineering University. Since 2007, she has been a Lecturer of College of Information and Communication Engineering at Harbin Engineering University. She is currently working at Katayama Lab of Nagoya University as a visiting scholar in Japan. Her current research interests include, Ultra Wideband Communication, Wideband Digital Communication System, and Communication Signal Processing.

Masaaki Katayama was born in Kyoto, Japan in 1959. He received the B.S., M.S. and Ph.D. degrees from Osaka University, Japan in 1981, 1983, and 1986, respectively, all in Communication Engineering. He was an Assistant Professor at Toyohashi University of Technology from 1986 to 1989, and a Lecturer at Osaka University from 1989 to 1992. In 1992, he joined Nagoya University as an associate professor, and has been a professor since July 2001. He is currently a vice-director of Institute of Materials and Systems for Sustainability, Nagoya University. He also had been working at the College of Engineering of the University of Michigan from 1995 to 1996 as a visiting scholar. His current research interests are on the physical and media-access layers of radio communication systems. His current research projects include, Smart Grid and Energy Management Systems, Wireless Sensing and Control, Cognitive Radio, Power-Line Communications, Visible Light Communications, Next Generation Mobile Communications, and Future Satellite Communications. He received the IEICE(was IECE) Shinohara Memorial Young Engineer Award in 1986, Distinguished Contributions Awards from Communications Society of IEICE three times in 1999, 2001, and 2006, and 2012 Outstanding Service Award from TC-PLC of IEEE. Dr. Katayama is a fellow and the chair of TC-Relialble Communication and Control of IEICE, and a senior member of IEEE.